

MAD on sky results in star oriented mode

Enrico Marchetti^{*a}, Roland Brast^a, Bernard Delabre^a, Rob Donaldson^a, Enrico Fedrigo^a, Christoph Frank^a, Norbert Hubin^a, Johann Kolb^a, Jean-Louis Lizon^a, Massimiliano Marchesi^a, Sylvain Oberti^a, Roland Reiss^a, Christian Soenke^a, Sebastien Tordo^a, Andrea Baruffolo^b, Paolo Bagnara^b, Antonio Amorim^c, Jorge Lima^c

^aEuropean Southern Observatory, Karl-Schwarzschild-Str. 2,
D-85748 Garching bei München, Germany;

^bOsservatorio Astronomico di Padova, vicolo dell'Osservatorio 5, I-35122 Padova, Italy;

^cUniversidade de Lisboa, Faculdade de Ciências, Campo Grande 1749-016, Lisbon, Portugal

ABSTRACT

The Multi-Conjugate Adaptive Optics Demonstrator (MAD) built by ESO with the contribution of two external consortia is a powerful test bench for proving the feasibility of Multi-Conjugate (MCAO) and Ground Layer Adaptive Optics (GLAO) techniques both in the laboratory and on the sky. MAD is based on a two deformable mirrors correction system and on two multi-reference wavefront sensors (Star Oriented and Layer Oriented) capable to observe simultaneously some pre-selected configurations of Natural Guide Stars. MAD corrects up to 2 arcmin field of view in K band. After a long laboratory test phase, it has been installed at the VLT and it successfully performed on-sky demonstration runs on several astronomical targets for evaluating the correction performance under different atmospheric turbulence conditions. In this paper we present the results obtained on the sky in Star Oriented mode for MCAO and GLAO configurations and we correlate them with different atmospheric turbulence parameters. Finally we compare some of the on-sky results with numerical simulations including real turbulence profile measured at the moment of the observations.

Keywords: Multi-Conjugate Adaptive Optics, Ground Layer Adaptive Optics, demonstrators

1. INTRODUCTION

Multi-Conjugate Adaptive Optics^{[1][2][3]} aims at performing wide field of view atmospheric turbulence correction using many Guide Stars (GSs) surrounding the observed target. The light coming from the GSs is analyzed through wavefront sensors whose signals are used to reconstruct the atmospheric turbulence at the different heights which some deformable mirrors are conjugated to.

Different approaches for MCAO correction have been proposed in the latest years such as the atmospheric tomography (also called Global Reconstruction) both in the zonal^[4] and in the modal way^[5] and the Layer Oriented one^{[6][7]}. The modal tomography has been also experimentally verified on the sky^[8]. These two approaches, in their basic concept, need different wavefront sensors (WFSs) in order to better optimize the appropriate atmospheric reconstruction.

The European Southern Observatory in collaboration with external research institutes has built an instrument prototype, the MCAO demonstrator^{[9][10]}, to prove on the sky the feasibility of the MCAO technique using both reconstruction approaches in the view of the future 2nd generation of the VLT instrumentation and the European Extremely large Telescope (E-ELT)^[11].

MAD has been installed at the VLT early in 2007 and performed the on-sky test runs starting from March 2007. In this paper, after recalling briefly the MAD system overview, we describe the observation methodology and the tools we used for data analysis. Then we proceed in discussing the results obtained in MCAO and GLAO configurations and we correlate them with the atmospheric parameters measured simultaneously during the observations. We will also show how the different repartition of the atmospheric turbulence in the high altitude layers affects the MCAO correction performance. Finally we will compare the observed results with the outcome of numerical simulations having as input the real turbulence profile obtained during the measurement of the selected cases.

* emarchet@eso.org, phone +49.89.32006458; fax +49.89.3202362; <http://www.eso.org/projects/aot/mad>

2. MAD OVERVIEW

MAD is a prototype MCAO system performing wide Field of View AO correction over 2 arcmin on the sky by using bright ($m_v < 13$) Natural Guide Stars (NGS).

It is implemented using existing technology and re-using as much as possible key components developed in the scope of existing ESO AO systems.

MAD will make use of two different wavefront sensors for implementing two independent wavefront correction techniques: the Star Oriented with a Shack-Hartmann WFS (SHWFS) sensing simultaneously 3 NGS with 3 SH WFS and the Layer Oriented with a Layer Oriented Wavefront Sensor (LOWFS) based on a Multi-Pyramid WFS^[12], sensing simultaneously 8 NGS. Each SHWFS samples the pupil with 8×8 sub-apertures, each one made by 8×8 pixels, for a total of 52 useful sub-apertures covering the full pupil. The SHWFS detectors are three CCD39 from E2V controlled by the ESO FIERA controller^[13]. The MAD Real-Time computer architecture is designed in order to support both wavefront sensors and reconstruction approaches.

The MAD correction is based on two bimorph deformable mirrors (DM), 60 actuators each, which are identical units of the ESO MACAO-VLTI^[14] and MACAO-SINFONI^[15] systems. One mirror is conjugated to the telescope pupil for ground layer turbulence correction, the second is conjugated at 8.5 Km above the telescope aperture, enabling a larger FoV correction. The MAD correction is optimized for the K ($2.2 \mu\text{m}$) band for the median Paranal seeing conditions and the performance are evaluated at this wavelength.

MAD uses a 1 arcmin FoV IR camera, called CAMCAO^[16], to evaluate the correction performance in the Near Infrared. The CAMCAO camera is mounted on a sliding device in order to patrol the 2 arcmin FoV for generating image mosaic covering the full MAD FoV.



Fig. 1. The MAD bench installed at the Nasmyth focal platform of the VLT unit telescope Melipal (UT3)

3. ANALYSIS TOOLS AND METHODOLOGY

During the MAD observations we simultaneously collected different types of data with the aim of post-processing and cross-correlating them after the end of the observation runs. To reduce and analyze the data we used different tools either developed appositely for MAD or available for general AO analysis purposes.

The data collected during MAD observations have been the following:

- CAMCAO images in K band (2.166 μm narrowband filter) over 1 arcmin (single exposure) or 2 arcmin FoV (mosaic of 5 images, 4 at corner and a central one) in closed and open loop. Equivalent skies, darks and flat fields have been obtained for images post-processing;
- DIMM^[17] real-time data, that is seeing and coherence time τ_0 , provided by the atmospheric monitor system of the Paranal observatory, together with the airmass at the moment of observation to reduce the above mentioned parameters to the line of sight;
- MASS^[18] real-time data, that is the atmospheric turbulence profile above the telescope at given altitudes: 562, 1125, 2250, 4500, 9000 and 18000m;
- SLODAR^[19] real-time data, that is the atmospheric turbulence profile measured with a resolution of 100m (variable) on 8 different altitude approximately within the first atmosphere's kilometer;
- Real-Time data files produced by the Real-Time computer during closed loop operations (wavefront sensor detector frames, centroid slopes, deformable mirror voltages); in the framework of this paper those data have been used more as closed loop quality check than for performance estimation, their reduction and analysis will be matter of a future work.

The CAMCAO images have been sky and dark subtracted, flat fielded and, where necessary, stitched to form the 2 arcmin FoV mosaic. The AO relevant parameters have been then extracted using the IDL based Strehl ratio meter routine already described in the previous MAD paper^[10] which first detects the stars present in an processed image, discards those outside the brightness user defined limits and having too close neighbors, then it delivers for each of them the Strehl ratio (SR), Encircled Energy (EE) and Full Width at Half Maximum (FWHM) in both axis, together with interpolated 2-D maps in the FoV for SR and FWHM. The SR, EE and FWHM values are given "as measured", that is, they include the uncorrected static aberrations present in MAD. The results are outputted in different formats for further use.

DIMM, MASS and SLODAR data are processed together to provide a detailed profile of the atmospheric turbulence at the moment of observations reduced for the line of sight. In the data analysis we used two vertical resolutions for the turbulence profile: a very coarse one, where we define as "ground" the turbulence below 500m and "altitude" the one above 500m, and a much more detailed one used to reproduce with numerical simulations (10 layers), the results obtained on the sky.

Finally the numerical simulations to reproduce the MAD on sky results have been implemented with an adaptive optics freeware numerical simulation tool called YAO developed by François Rigaut^[20] developed in Yorick environment and running on Linux platforms. This numerical tool is extremely flexible and allows simulating a large variety of configurations including MCAO systems.

4. MCAO AND GLAO ON SKY RESULTS

The object we observed the most during the MAD technical run was Omega Centauri, a very crowded globular cluster, having GSs bright enough and in comfortable asterism shapes to close the AO loops, and to find a uniform angular repartition of bright stars in the field to compute SR and FWHM maps over the 2 arc minutes FoV. The results described in this papers have been obtained during the MAD observations carried out in the period March 25th – April 5th 2007.

Once selected the suitable GS asterism (three GSs on an equilateral triangle of 1.8 arcmin diameter, with $m_v \sim 11.5$) we proceeded with their acquisition and with the recording of the interaction matrix directly on the sky with fast Hadamard calibration method^[21]. The reconstructor has been computed by simple SVD inversion of the interaction matrix filtering

out the systems modes with the highest propagated error. The number of filtered modes has been experimentally obtained by a dedicated optimization run on sky executed before the systematic performance measurement campaign.

The images have been obtained using CAMCAO and Bracket- γ narrowband filter at 2.166 μm , the total equivalent exposure time for each image set to 60s (DIT=10s, NDIT=6). When 2 arcmin FoV has been observed, the related mosaic (5 images) has been obtained by moving CAMCAO to scan the FoV and maintaining the AO loop closed.

After a quick check of closing loop capability in Single Conjugated configuration, we started the performance measurement closing alternately the MCAO and the GLAO loops. This was achieved by exchanging the related control matrices. Values for the integral loop gain have been set accordingly to the optimization run executed previously. In the mean time we continuously recorded the atmospheric turbulence parameters which were evolving during the observations.

We decided to perform two kinds of observations:

- Central square arcmin FoV which requires faster total exposure time with respect to the 2 arcmin mosaic (5 times more time consuming) enabling us to collect a noticeable number of consecutive images and providing a significant statistical coverage of different seeing conditions; on the other side the central arcmin is not fully representative of the global GLAO and MCAO correction capabilities in the full FoV since the results are biased by the fact that the central region MCAO is the configuration which benefits the less and GLAO is the one which benefits the more;
- Full 2 arcmin FoV which requires a mosaic of 5 images thus more expensive in time to acquire; in this case the different behaviors between MCAO and GLAO are more evident but the atmospheric statistics spanned when observing such a FoV came out to be poor; moreover, depending on the atmospheric variability, the consistency of the correction in the field could be corrupted by the fact that different tiles of the mosaic could be acquired under different atmospheric turbulence conditions.

In Fig. 2 and Fig. 3 are shown the typical close loop correction behaviors for MCAO and GLAO at 2.166 μm under good seeing conditions. In the case of MCAO the correction is pretty flat in over the full 2 arcmin FoV and it peaks around the directions of the GS. In the specific case of Fig. 2 the intermediate/high levels of Strehl ratio guarantee a quite uniform FWHM across the FoV.

As expected for GLAO correction is lower than in MCAO, limited to the triangle formed by the GS and not significantly peaked on those. In the specific case of Fig. 3 the levels of Strehl are low and the final FWHM in drops quickly outside the GS triangle.

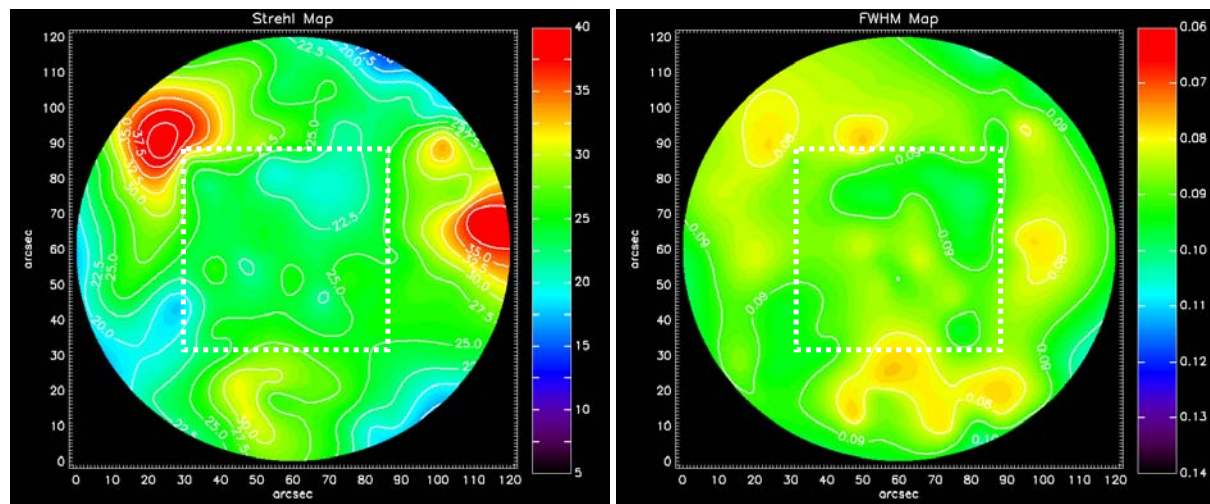


Fig. 2. Typical MCAO close loop correction behavior in the 2 arcmin FoV at 2.166 μm ; left: SR map (%), right FWHM map (arcsec). The central arcmin is also displayed.

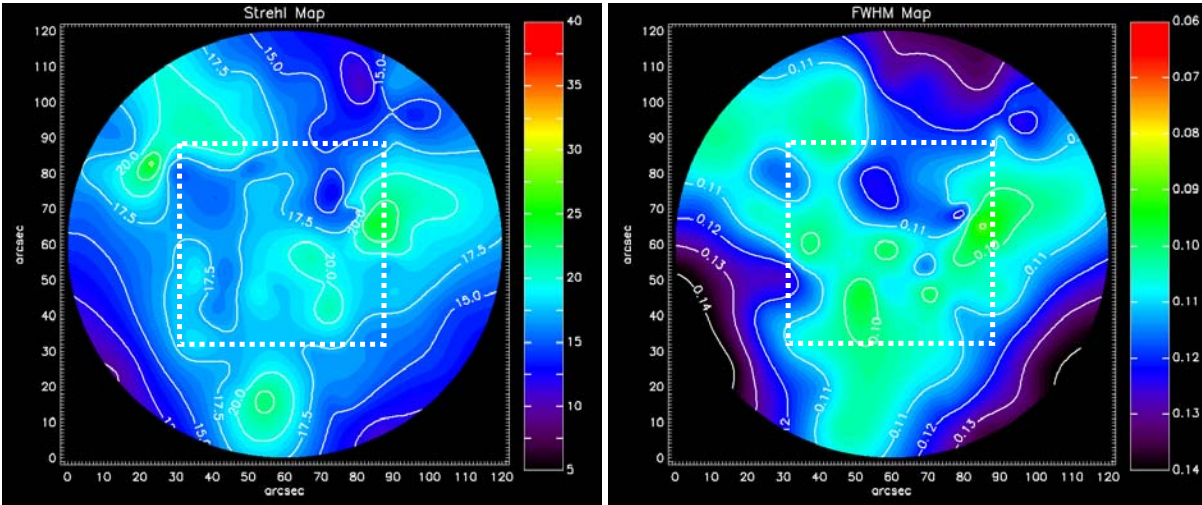


Fig. 3. Typical GLAO close loop correction behavior in the 2 arcmin FoV at 2.166 μm ; left: SR map (%), right FWHM map (arcsec). The central arcmin is also displayed

4.1 Performance vs. atmospheric turbulence conditions

We first correlate the average Strehl Ratio with the seeing in the line of sight. In Fig. 4 is shown the corresponding plot including for both the central arcmin and the 2 arcmin FoV. It is worth mentioning that Strehl values below 5% have a very high intrinsic error. It is evident the general trend of the performance decreasing when the seeing worsens. MCAO has better performance than GLAO for good seeing conditions ($<0.8''$) while at intermediate and bad seeing conditions this difference is not anymore so obvious. The best average Strehl for MCAO at good seeing conditions ($<0.8''$) is $\sim 22\text{--}23\%$ in the central arcmin and $\sim 25\%$ in the 2 arcmin; GLAO best average Strehl is $\sim 17\text{--}18\%$ in the central arcmin and $\sim 15\%$ in the 2 arcmin. This is consistent with the fact that MCAO corrects better at the edge of FoV than GLAO.

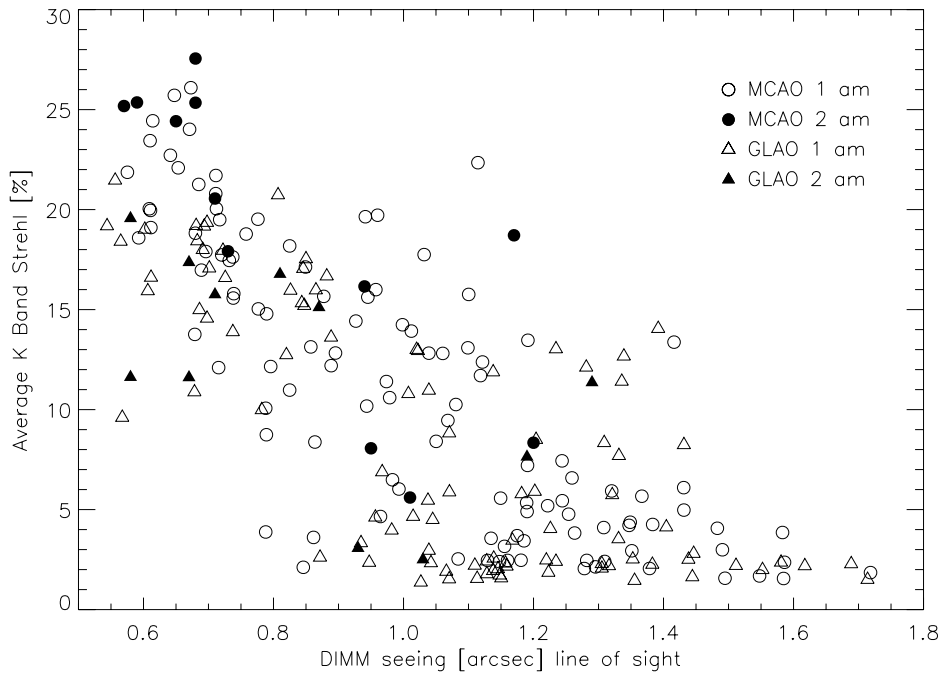


Fig. 4. Average K band SR in the specified FoV vs. the DIMM seeing in the line of sight.

As mentioned previously, the performances of GLAO and MCAO don't depend only on the turbulence strength, but also on the repartition in altitude of the turbulent layers. The MASS-DIMM combined measurements allow retrieving at each moment the fraction of the turbulence present above and below 500m above the telescope. It is possible to plot the performance of the system vs. fraction of turbulence above 500m (Fig. 5).

MCAO holds significant correction performance when the fraction of altitude turbulence is larger than 40% while GLAO maintains efficient correction only in presence of important ground layer (>60%). The MCAO points with low average SR at strong altitude turbulence refer mostly to bad seeing conditions, while this is not true for GLAO. In the plot there is an intrinsic bias for which good seeing is always coupled with strong ground layer (see Fig. 7); from this situation GLAO benefits having only the DM at ground compensating for turbulence and this explains why GLAO performance is surprisingly close the MCAO one. In Fig. 4 few GLAO points show an unexpected high average Strehl in intermediate seeing conditions (~12-14% between 1.2'' and 1.4''); this apparent anomaly is explained by the fact that those points have been obtained in presence of a very strong ground layer as in Fig. 5 they are all shifted around 20% of altitude turbulence. The 2 arcmin data have been obtained only at intermediate-good seeing conditions when the ground layer is always strong and they obviously don't show a significant trend as the central arcmin data.

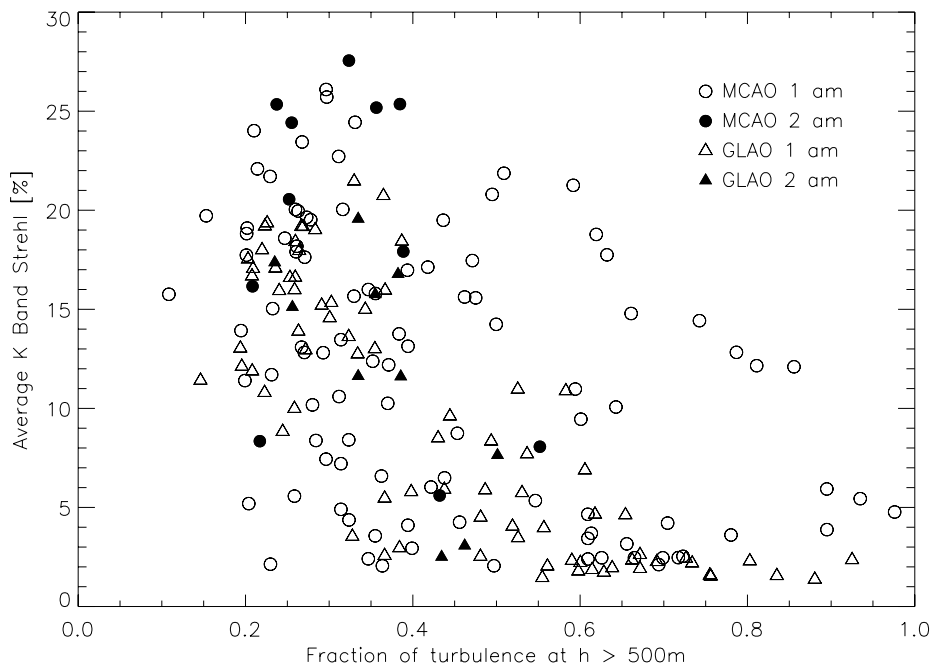


Fig. 5. Average K band SR in the specified FoV vs. fraction of turbulence above 500 m.

It is possible to repeat the analysis using the FWHM instead of the SR. Since these two quantities are somehow directly linked, these two new plots don't bring additional information about the correction performance of GLAO and MCAO with respect the SR but for sake of clarity we show, as an example, the average FWHM vs. the fraction of turbulence above 500 m (Fig. 6). In the central arcmin with altitude turbulence contribution <40% the difference between MCAO and GLAO are similar to the case of good seeing, then with increasing altitude turbulence contribution MCAO holds a significant performance while GLAO degrades; the behavior is the same but stronger for the 2 arcmin. The few bad (large FWHM) MCAO points at altitude turbulence contribution <40% refer to bad seeing conditions.

For information completion the trend of the FWHM vs. seeing (plot not shown here), in the central arcmin up to ~1.0'' seeing MCAO average FWHM (~0.09''-0.1'') is similar or slightly better than for GLAO, at worse seeing GLAO performance quickly degrades while MCAO still holds an acceptable correction. In the 2 arcmin up to ~1.0'' seeing MCAO (~0.08''-0.09'') is always ~0.02'' better than GLAO (~0.11''); this is consistent with the fact that MCAO corrects better at the edge of FoV than GLAO, at worse seeing GLAO becomes much worse than MCAO at least by a factor 2.

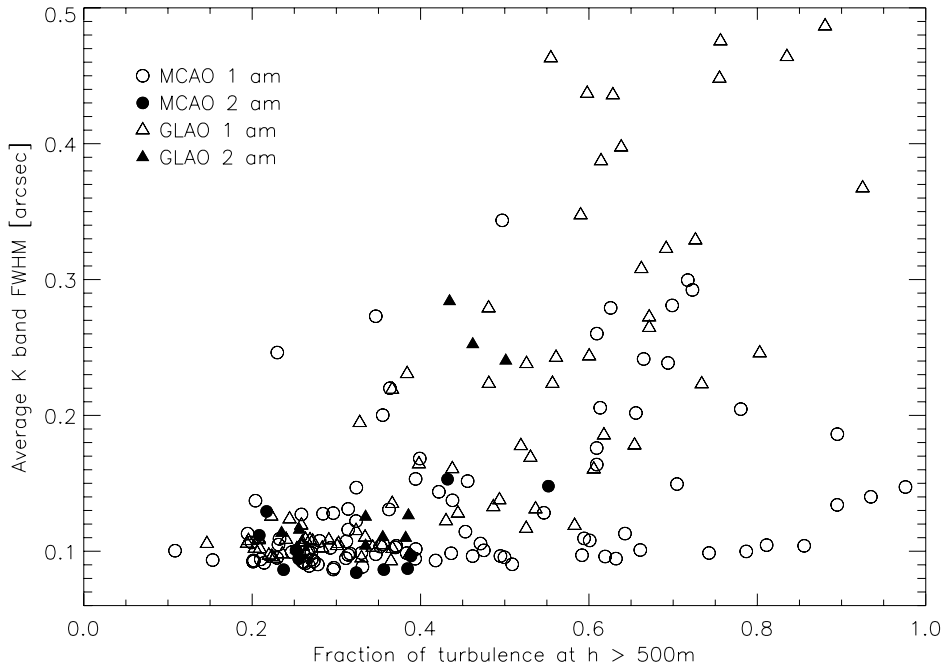


Fig. 6. Average K band FWHM in the specified FoV vs. fraction of turbulence above 500 m.

Finally another relevant parameter to study is the uniformity of the correction in the FoV. The Fig. 8 shows the FWHM RMS in the central arcmin and in the 2 arcmin as a function of the average FWHM.

For high correction performance (FWHM $\sim 0.1''$) MCAO and GLAO have similar RMS and this is likely a linear function of the average FWHM: the better the correction the better the uniformity. When the correction degrades GLAO exhibits a faster stabilization at values smaller than the ones experienced by MCAO. This behavior can be explained by the fact that in poor seeing conditions MCAO still corrects somehow efficiently in the direction of the guide stars while GLAO doesn't; this excess of correction transfers into a lower uniformity for MCAO.

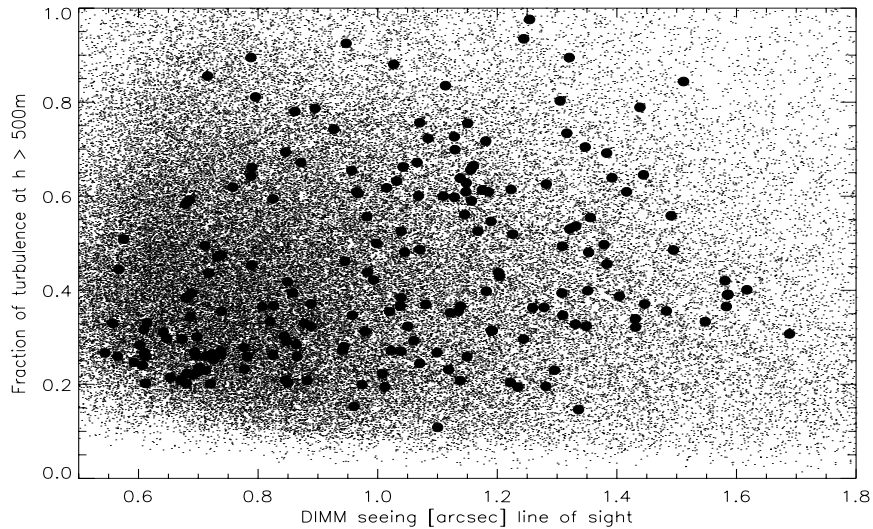


Fig. 7. Distribution of fraction of altitude turbulence ($>500\text{m}$) vs. DIMM seeing during MAD observations (big circles) compared to the typical yearly one of Paranal (dots).

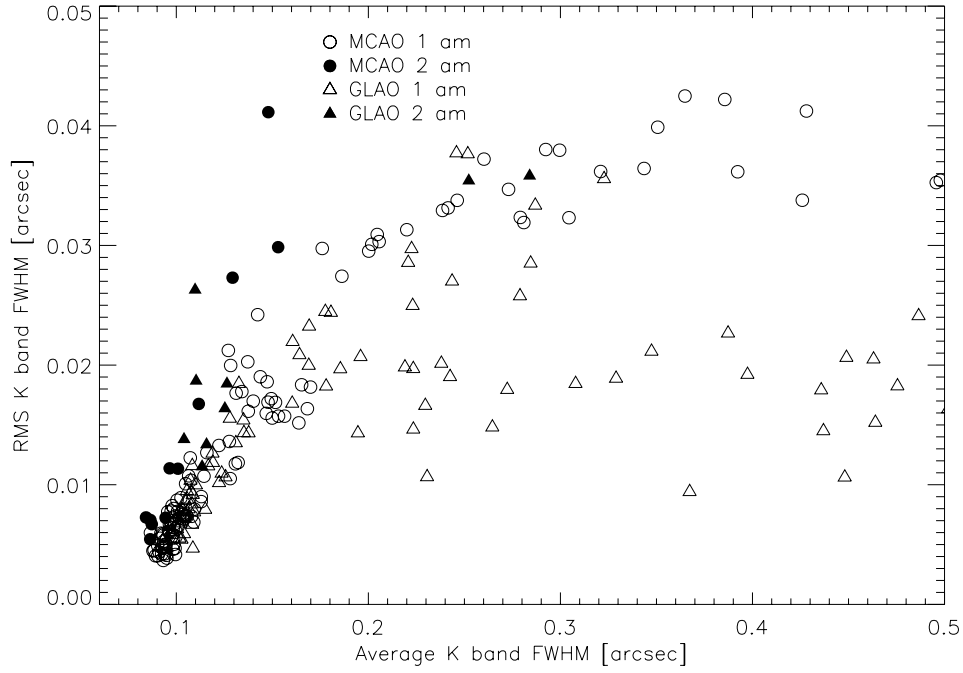


Fig. 8. RMS of K band FWHM vs. the average FWHM in the specified FoV.

4.2 Effect of turbulence profile change

It has been shown that the coarse repartition of the vertical distribution of the turbulence between ground layer (<500 m) and altitude turbulence (> 500 m) provides already a good understanding of the physics behind for the GLAO and MCAO correction. In this section we want to explore more in detail the effects of the vertical distribution of the turbulence on MCAO using the data collected during the MAD on-sky runs.

In Fig. 9 are shown two Strehl maps obtained under very similar seeing conditions in terms of DIMM seeing, coherence time and fraction of altitude turbulence but having different strength repartition within the altitude turbulence. The turbulence parameters for the two Strehl maps are listed in Table 1:

Parameters	High Strehl (left)	Low Strehl (right)
DIMM Seeing (line of sight)	0.68''	0.71''
τ_0	3.0 ms	3.3 ms
Altitude turb. (> 500m)	0.39	0.34
0.5 km < h < 9 km (rel.)	74%	55%
9 km < h < 13.5 km (rel.)	14%	25%
h > 13.5 km (rel.)	12%	20%

Table 1. Relevant atmospheric parameters for the two MCAO correction cases considered in this section.

The left-hand side Strehl map, having good correction, has been obtained when most of the altitude turbulence (74%) was concentrated between the two deformable mirrors (0.5 km < h < 9 km). Both DMs are not correcting only the layer they are conjugated to, but they have also a “depth” of correction which is less efficient moving far from conjugation altitude but still partially effective. The turbulence in between the DMs benefits from this partial correction and it gets attenuated increasing in this way the average Strehl. The right-hand side Strehl map has been obtained in similar “macroscopic” seeing conditions but with a distribution of the altitude turbulence less favorable for efficient correction.

In fact a significant part of the altitude turbulence (44%) is located above or much above the upper DM and this reduces the capability of correction of the system. Moreover the effect is amplified by the projected lower spatial resolution of the upper DM's actuators.

This example shows that the MAD system and likely any MCAO system in general are sensitive to more turbulence parameters than the single AO systems and those have to be taken into account when providing estimation of correction during a design study phase.

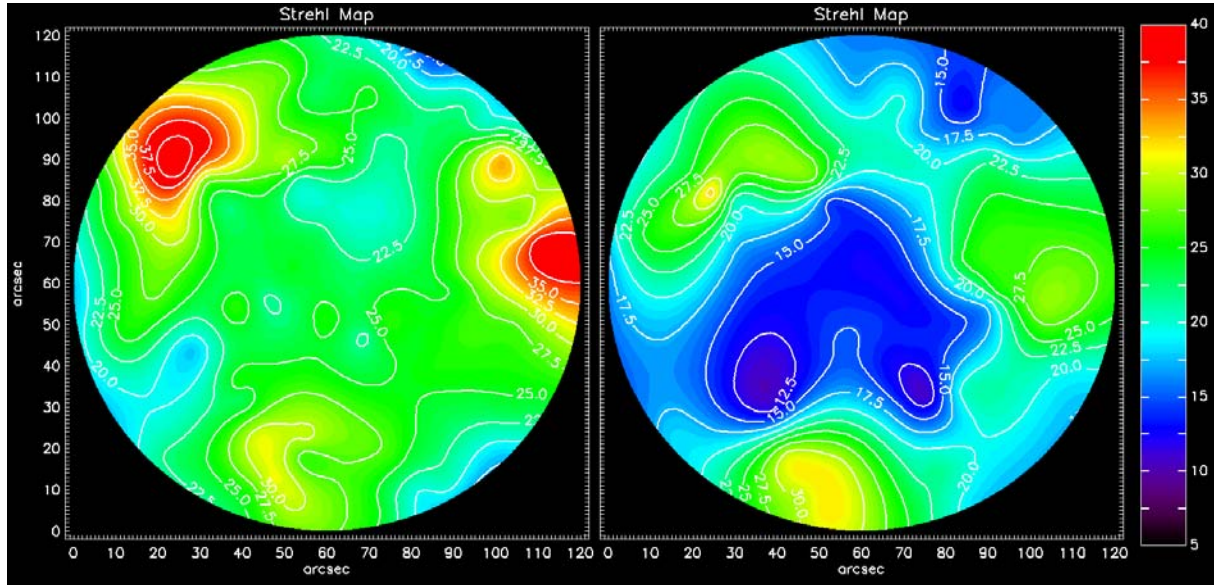


Fig. 9. MCAO Strehl maps obtained for similar conditions of DIMM seeing, coherence time and fraction of altitude turbulence (>500 m). The left map has been obtained when more than 74% of the altitude turbulence concentrated between the conjugation altitudes of the two DMs (< 9 km). For the right map 45% of the turbulence was located above the upper DM.

5. SIMULATING REAL CASES

In this section we present the numerical simulation results aiming at reproducing some of the most relevant results obtained with MAD on sky in the MCAO and GLAO configurations.

The simulation input parameters have been set in order to reproduce as close as possible the MAD system some of them being experimentally measured during the calibrations after the installation of the system at VLT. Among the several inputs the most relevant one are: Von-Karman turbulence with $L_0=22$ m, full wavefront sensor model including measured noise sources, bimorph deformable mirrors, two-step delay servo-loop, reconstructor from truncated SVD, MAD static aberrations not corrected by AO closed loop.

5.1 Turbulence profiles

The DIMM, MASS and SLODAR measurements have been combined together to provide the turbulence strength at different altitudes. Due to fast temporal fluctuation of the MASS and SLODAR values, a 10 minutes average has been computed and then the turbulence profile has been restructured in 10 layers (0, 300, 900, 1800, 4500, 7100, 11000, 12800 and 16500m) in order to homogenize it with the actual simulation baseline defined at ESO for the E-ELT. From the same baseline we adopted the values for the wind speed at the different altitudes and scaled them in order to match the τ_0 value at the moment of the observation. It is worth noting that the process of recording a 2 arcmin mosaic (5 images) was taking about 6 minutes and during this time the seeing and τ_0 were often varying. In the simulations we considered only the average of those variations which brings a not negligible level of uncertainty on the results and it is pushing us to be cautious when comparing measurement on the sky (with variable conditions) and simulations.

Hereafter we consider three cases: the two MCAO of Sec. 4.2 and the GLAO of Sec. 4.1.

5.2 MCAO and GLAO simulations vs. measured performance

The results of the simulations are given in Fig. 10, Fig. 11 and Fig. 12. The only parameter we changed in order to find the best fit with the observed results has been the value of the seeing. We have found a good matching for both the MCAO cases and the GLAO one within the range of the seeing variation during observation.

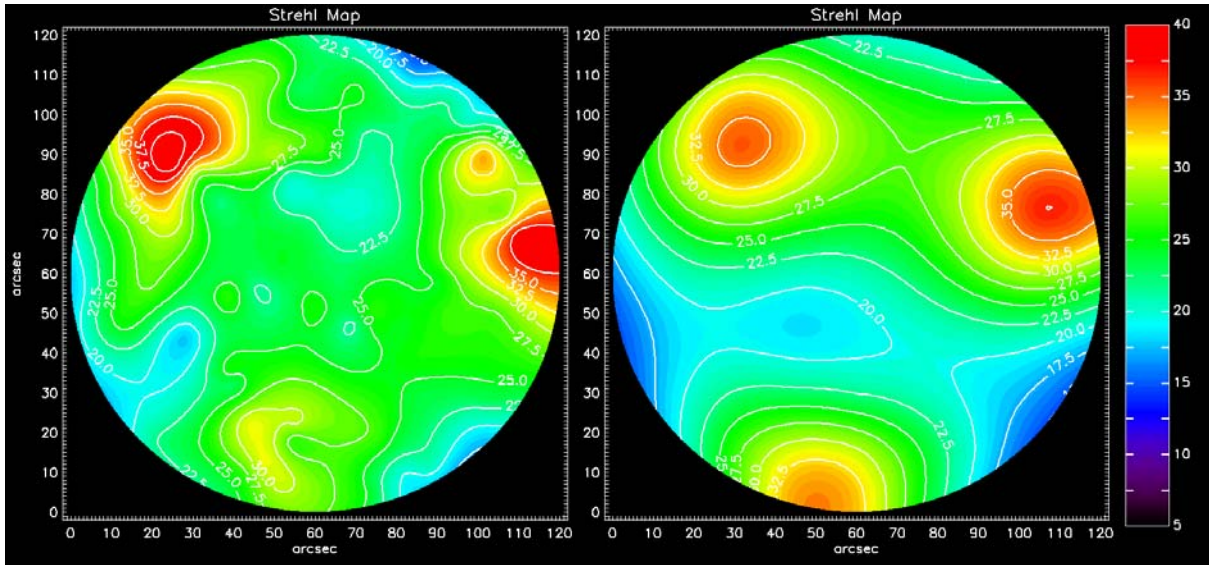


Fig. 10. MCAO SR maps in K band for the “good” turbulence profile of Sec. 4.2. Left: measured on sky. Right: simulated with average seeing on the line of sight of $0.72''$ ($0.04''$ more than nominal value). During the observation the seeing varied by $0.05''$ (PTV).

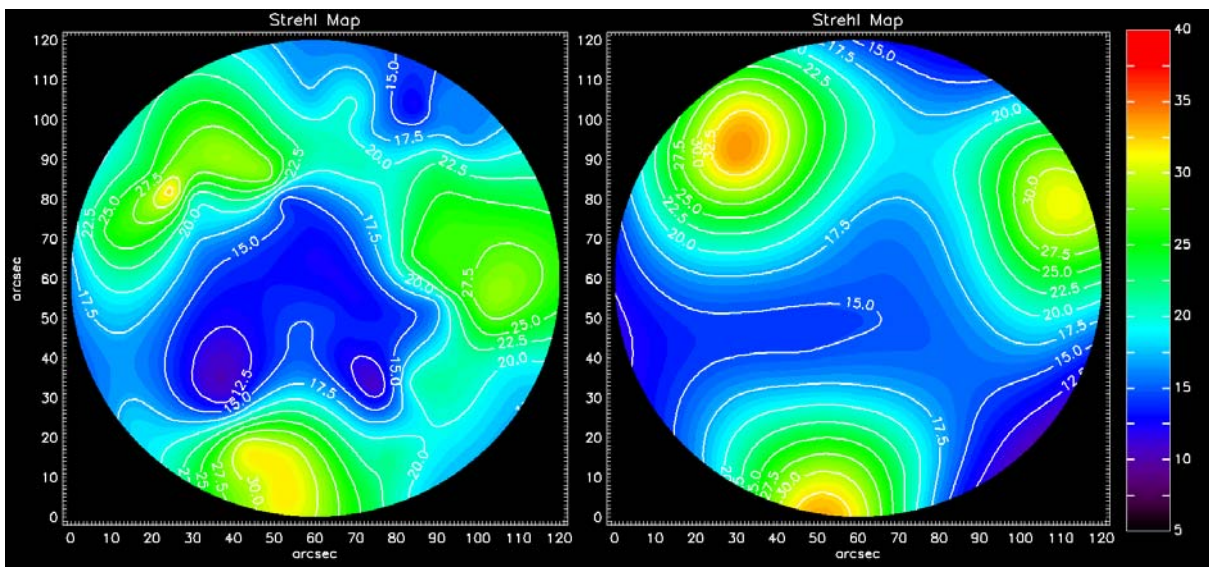


Fig. 11. MCAO SR maps in K band for the “bad” turbulence profile of Sec. 4.2. Left: measured on sky. Right: simulated with average nominal seeing on the line of sight of $0.63''$. During the observation the seeing varied by $0.08''$ (PTV).

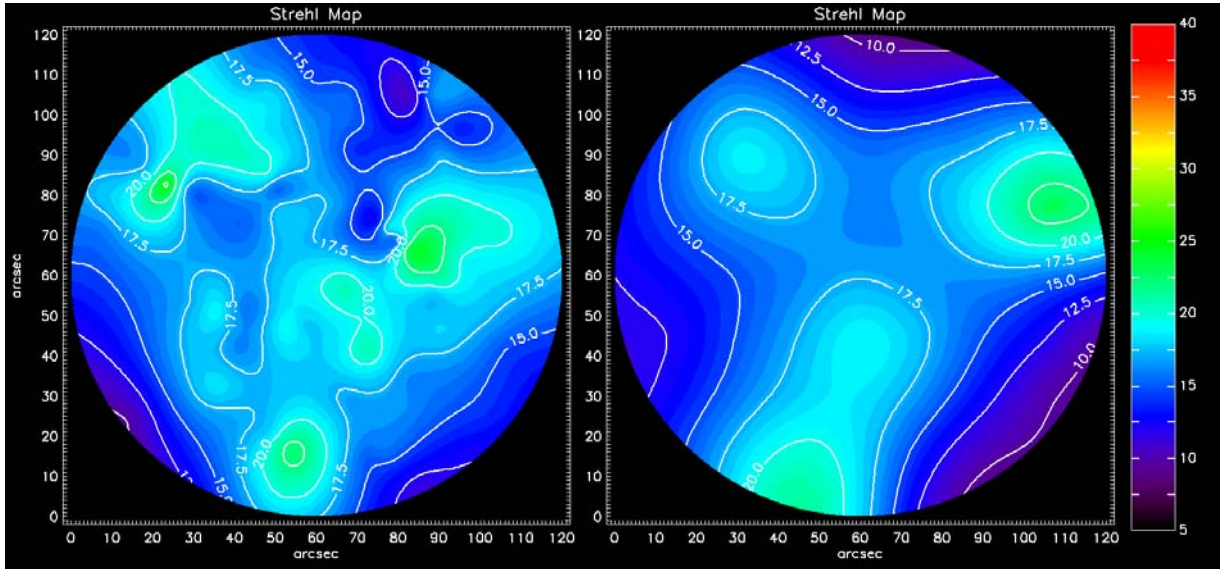


Fig. 12. GLAO SR maps in K band for the case of Sec.4.1. Left: measured on sky. Right: simulated with average seeing on the line of sight of $0.63''$ ($0.04''$ less than the nominal value). During the observation the seeing varied by $0.04''$ (PTV).

6. CONCLUSIONS

During the on-sky test run of March 2007 the seeing conditions have been widely ranging from good to bad allowing to scan efficiently the turbulence parameters space. As a peculiarity we observed a trend for turbulence vertical distribution which is opposite to the yearly average in Paranal: we experienced that good seeing conditions are associated with a relative strong ground layer while for bad seeing the occurrence of important ground layer less evident. The median contribution value for is around 60% of the total turbulence.

MCAO and GLAO have been extensively compared vs. seeing conditions using the globular cluster Omega Centauri as crowded field. The performance has been estimated for an asterism on 2 arcmin diameter in order to privilege the study of the correction behavior at the maximum distance from the GSs. As a general trend the better is the seeing the better the correction. Strehl performance is poor above 1.5 arcsec seeing, but still a FWHM improvement has been observed. As expected GLAO correction peaked at the FoV center while MCAO is peaked on the guide stars. MCAO has always better performance in the FoV while GLAO for good seeing condition is close to MCAO in the central arcmin. This result is not surprising since our observations were systematically biased by peculiar (i.e. not statistically typical for Paranal) atmospheric turbulence conditions. In fact good seeing conditions were always associated to strong ground layer (up to 80%), a situation for which GLAO shows its strength. On the contrary as soon as the ground layer loses power GLAO performance drop quickly while MCAO still provides good correction under same seeing conditions. Performances in FWHM follow closely the ones for the Strehl. The correction uniformity exhibits a different trend: MCAO and GLAO are identically uniform under good seeing conditions but as soon as the turbulence gets stronger MCAO worsen in uniformity faster than GLAO. This behavior can be explained by the fact that in poor seeing conditions MCAO still corrects somehow efficiently in the direction of the guide stars, thanks to the upper DM, while GLAO doesn't, producing high variability of correction in the FoV, thus the lower uniformity.

Vertical distribution of the altitude turbulence plays an important role in the capability for MCAO to perform efficient correction. When most of turbulence is located in between the two DMs the correction provides higher Strehl than when the turbulence is spread above the upper DM. This can be explained by the fact that both DMs are not correcting only the layer they are conjugated to, but they have also a "depth" of correction which is less efficient moving far from conjugation altitude but still partially effective.

We performed extensive simulations to reproduce the results obtained on the sky with MCAO and GLAO. Using simultaneous real time atmospheric data we have been able to fully reconstruct the vertical distribution of turbulence at the time of observations and to implement in the numerical code a 10 layers atmospheric model suitable for our

purposes. We have been able to reproduce both MCAO and GLAO performance, the earlier also for change of vertical distribution of turbulence, with an accuracy which is in the range of the variation of the seeing during the observations.

REFERENCES

- [1] Beckers, J. M., “Increasing the size of the isoplanatic patch size with multiconjugate adaptive optics”, in ESO conference on Very Large Telescopes and their instrumentation, M.-H. Hulrich, ed., 693 (1988).
- [2] Beckers, J. M., “Detailed compensation of atmospheric seeing using multiconjugate adaptive optics”, Proc. SPIE 1114, 215-217 (1989).
- [3] Ellerbroek, B., “First order performance evaluation of adaptive optics system for atmospheric turbulence compensation in extended field-of-view astronomical telescope”, JOSA A 11, 783-805 (1994).
- [4] Tallon, M. and Foy, R., “Adaptive telescope with laser probe - Isoplanatism and cone effect”, A&A 235, 549-557 (1990).
- [5] Ragazzoni, R., Marchetti, E., Rigaut, F., “Modal tomography for adaptive optics”, A&A 342, L53-L56 (1999).
- [6] Ragazzoni, R., “Adaptive optics for giants telescopes: NGS vs. LGS”, in ESO Proceedings of the Bäckaskog Workshop on Extremely large Telescopes 57, T. Andersen, A. Ardeberg and R. Gilmozzi, eds., 175-180 (2000).
- [7] Ragazzoni, R., Farinato, J., Marchetti, E., “Adaptive optics for 100-m-class telescopes: new challenges require new solutions”, Proc. SPIE 4007, 1076-1087 (2000).
- [8] Ragazzoni, R., Marchetti, E., Valente, G., “Adaptive-optics correction available for the whole sky”, Nature 403, 54-56 (2000).
- [9] Marchetti, E., Brast, R., Delabre, B., Donaldson, R., Fedrigo, E., Frank, C., Hubin, N., Kolb, J., Lizon, J.-L., Marchesi, M., Oberti, S., Reiss, R., Santos, J., Soenke, C., Tordo, S., Baruffolo, A., Bagnara, P., The CAMCAO Consortium “On-sky Testing of the Multi-Conjugate Adaptive Optics Demonstrator”, The Messenger 129, 9-13 (2007).
- [10] Marchetti, E., Brast, R., Delabre, B., Donaldson, R., Fedrigo, E., Frank, C., Hubin, N., Kolb, J., Le Louarn, M., Lizon, J.-L., Oberti, S., Quirós-Pacheco, F., Reiss, R., Santos, J., Tordo, S., Baruffolo, A., Bagnara, P., Amorim, A., Lima, J., “MAD Star Oriented: laboratory results for Ground Layer and Multi-Conjugate Adaptive Optics”, Proc. SPIE 6272, 00 (2006).
- [11] Gilmozzi, R., Spyromilio, J., “The European Extremely large Telescope (E-ELT)”, The Messenger 127, 11-19 (2007).
- [12] Ragazzoni, R., “Pupil plane wave front sensing with an oscillating prism”, J. of Mod. Opt. 43, 289-293 (1996).
- [13] Beletic, J. W., Gerdes, R., Duvarney, R.C., “Fiera: ESO's New Generation CCD Controller”, ExA 8, 13-24 (1998).
- [14] Arsenaault, R., Donaldson, R., Dupuy, C., Fedrigo, E., Hubin, N.H., Ivanescu, L., Kasper, M.E., Oberti, S., Paufique, J., Rossi, S., Silber, A., Delabre, B., Lizon, J.-L., Gigan, P., “MACAO-VLTI Adaptive Optics System Performance”, Proc. SPIE 5490, 47-58 (2004).
- [15] Bonnet, H., Conzelmann, R.D., Delabre, B., Donaldson, R., Fedrigo, E., Hubin, N.H., Kissler-Patig, M., Lizon, J.-L., Paufique, J., Rossi, S., Stroebele, S., Tordo, S., “First Light of SINFONI AO Module at VLT”, Proc. SPIE 5490, 130-138 (2004).
- [16] Amorim, A., Lima, J., Alves, J., Rebordão, J., Pinhão, J., Gurriana, L., Cabral, A., Marchetti, E., Kolb, J., Tordo, S., Finger, G., Lizon, J.-L., Santos Duarte, F., Marques Ferreira, R., Alves, R., Barros, R., “Integration and first results of the CAMCAO NIR camera”, Proc. SPIE 6269, 57 (2006).
- [17] Sarazin, M., Roddier, F., “The ESO differential image motion”, A&A 227, 294-300 (1990).
- [18] Kornilov, V., Tokovinin, A., Vozyakova, O., Zaitsev, A., Shatsky, N., Potanin, S.F., Sarazin, M., “MASS: a monitor of the vertical turbulence distribution”, Proc. SPIE 4839, 837-845 (2003).
- [19] Wilson, R.W., “SLODAR: measuring optical turbulence altitude with a Shack-Hartmann wavefront sensor”, MNRAS 337, 103-108 (2002).
- [20] Rigaut, F., web page: <http://www.maumae.net/yao>
- [21] Kasper, M., Fedrigo, E., Looze, D.P., Bonnet, H., Ivanescu, L., Oberti, S., “Fast calibration of high-order adaptive optics systems”, JOSA A 21, 1004-1008 (2004).